*Cerebral Cortex*, March 2017;27:2418–2433

**doi:10.1093/cercor/bhw102**
Advance Access Publication Date: 19 April 2016
Original Article

ORIGINAL ARTICLE

# In Vitro Corticogenesis from Embryonic Stem Cells Recapitulates the In Vivo Epigenetic Control of Imprinted Gene Expression

Tristan Bouschet[1], Emeric Dubois[2], Christelle Reynès[1], Satya K. Kota[3], Stéphanie Rialle[2], Stéphanie Maupetit-Méhouas[4], Mikael Pezet[1], Anne Le Digarcher[1], Sabine Nidelet[2], Vincent Demolombe[2], Patricia Cavelier[3], Céline Meusnier[1], Chloé Maurizy[1,3], Robert Sabatier[1], Robert Feil[3], Philippe Arnaud[4], Laurent Journot[1,2] and Annie Varrault[1]

[1]Institut de Génomique Fonctionnelle (IGF), CNRS UMR5203, INSERM U1191, Université de Montpellier, Montpellier, France, [2]Montpellier GenomiX, BioCampus Montpellier, CNRS UMS3426, INSERM US009, Université de Montpellier, Montpellier, France, [3]Institute of Molecular Genetics (IGMM), CNRS UMR 5535, University of Montpellier, Montpellier, France and [4]GReD (Genetics, Reproduction and Development), CNRS UMR6293, INSERM U1103, Université Clermont Auvergne, Clermont-Ferrand, France

Address correspondence to Tristan Bouschet. Email: tristan.bouschet@igf.cnrs.fr; Annie Varrault. Email: annie.varrault@igf.cnrs.fr

## Abstract

In vitro corticogenesis from embryonic stem cells (ESCs) is an attractive model of cortical development and a promising tool for cortical therapy. It is unknown to which extent epigenetic mechanisms crucial for cortex development and function, such as parental genomic imprinting, are recapitulated by in vitro corticogenesis. Here, using genome-wide transcriptomic and methylation analyses on hybrid mouse tissues and cells, we find a high concordance of imprinting status between in vivo and ESC-derived cortices. Notably, in vitro corticogenesis strictly reproduced the in vivo parent-of-origin-dependent expression of 41 imprinted genes (IGs), including *Mest* and *Cdkn1c* known to control corticogenesis. Parent-of-origin-dependent DNA methylation was also conserved at 14 of 18 imprinted differentially methylated regions. The least concordant imprinted locus was *Gpr1-Zdbf2*, where the aberrant bi-allelic expression of *Zdbf2* and *Adam23* was concomitant with a gain of methylation on the maternal allele in vitro. Combined, our data argue for a broad conservation of the epigenetic mechanisms at imprinted loci in cortical cells derived from ESCs. We propose that in vitro corticogenesis helps to define the still poorly understood mechanisms that regulate imprinting in the brain and the roles of IGs in cortical development.

**Key words:** allele-specific expression, corticogenesis, DNA methylation, embryonic stem cells, genomic imprinting

## Introduction

It is likely that neocortical neurogenesis in humans (Bhardwaj et al. 2006) and mice (Ehninger and Kempermann 2003) are restricted to the developmental period. Promising sources of neurons to repair the damaged adult cortex are cortical-like cells obtained in vitro through selective differentiation of mouse (Eiraku et al. 2008; Gaspard et al. 2009) or human (Shi et al. 2012; Espuny-Camacho et al. 2013) ESCs. To which extent in vitro corticogenesis recapitulates the in vivo process is an important issue that is highly debated (Lancaster and Knoblich 2014; Livesey et al. 2015). In light of the biological parameters that have

been measured so far, in vitro cortical-like cells from ESCs seem a worthy source of cells for cortical therapy and a valuable model system for corticogenesis. In vitro corticogenesis from ESCs notably reproduces the temporal expression of markers of cortical layers and projections of axons upon grafting into a recipient mouse cortex (Eiraku et al. 2008; Gaspard et al. 2008; Hansen et al. 2011; Espuny-Camacho et al. 2013). In addition, ESC-derived cortical cells grafted in the visual cortex respond to visual stimuli (Michelsen et al. 2015), suggesting that these cells could functionally reconstitute a damaged cortical circuit.

A remaining concern and unanswered issue about in vitro cortex is its epigenetic signature. During development, the generation of a comprehensive repertoire of differentiated cells parallels a complex reorganization of the epigenetic landscape (Thiagarajan et al. 2014). Changes in the epigenetic signature orchestrate the regulation of developmental genes such as *Neurogenin1* in the developing cortex (Hirabayashi et al. 2009). Mutations in the epigenetic machinery lead to specific neurodevelopmental diseases (Jakovcevski and Akbarian 2012). In vitro culture can also alter DNA methylation patterns (Lund et al. 2012; Cahan and Daley 2013; Thiagarajan et al. 2014). Hence, a major hurdle for the use of ESCs in cortical development studies and cortical therapy is to prove that ESC-derived cortical cells reproduce the epigenetic signature of the in vivo cortex.

The so-called imprinted genes (IGs) are particularly relevant in this context as they display allele-specific expression depending on the epigenetic status of both parental genomes and many are involved in corticogenesis. Parental genomic imprinting is an epigenetic mechanism that restrains the expression of approximately 140 IGs in mouse and human to one parental allele (Kelsey and Feil 2013). This parent-of-origin-dependent expression is due to methylation marks deposited on *d*ifferentially *m*ethylated DNA regions (DMRs) during female and male gametogenesis that distinguish the genomes inherited from the mother and the father (Ferguson-Smith 2011; Kelsey and Feil 2013). For example, at the *Dlk1-Dio3* imprinted locus, methylation is restrained to the paternal DMR and neighboring IGs are exclusively expressed either from the paternal (*Dlk1* and *Rtl1*) or from the maternal (*Meg3* and *Mirg*) allele (Ferguson-Smith 2011; Kelsey and Feil 2013). Depending on tissue and developmental stage, a given IG is expressed exclusively from one parental allele, expressed preferentially from one parental allele with an incomplete silencing of the normally repressed allele, or expressed equally from both parental alleles (Prickett and Oakey 2012; Bonthuis et al. 2015). Brain is a known hotspot for tissue-specific imprinting (Prickett and Oakey 2012), as recently confirmed by RNA-seq experiments on F1 hybrid whole brain (Wang et al. 2008, 2011; DeVeale et al. 2012; Babak et al. 2015). For instance, *Ube3a*, whose loss of function results in Angelman syndrome, is bi-allelically expressed in most organs, while it is maternally expressed in neurons (Albrecht et al. 1997; Chamberlain and Lalande 2010). Moreover, some IGs play a key role in cortical development: *Cdkn1c* and *Igf2* regulate progenitor proliferation (Lehtinen et al. 2011; Mairet-Coello et al. 2012; Tury et al. 2012) and *Dlk1* regulates neurogenesis in the postnatal niche (Ferron et al. 2011). *Mest* mutant mice display alteration of motor cortex patterning (Sansom et al. 2005). IGs are also involved in human corticogenesis. Microcephaly (Mueller and Coovadia 2008) or hypoplasia of the corpus callosum (Mackay et al. 2008) has been observed in some patients with imprinting disorders. Imprinting can be affected by the process of culturing cells and organs in vitro (Dean et al. 1998; Lund et al. 2012) and the maintenance of genomic imprints is therefore commonly used to evaluate epigenetic stability during cell culture, notably in ESCs and their derivatives (Dean et al. 1998; Pick et al. 2009; Lund et al. 2012; Ficz et al. 2013; Greenberg and Bourc'his 2015; Stelzer et al. 2015). Nevertheless, the parent-of-origin-dependent gene expression and methylation of all the murine imprinted loci in the cerebral cortex generated both in vivo and in vitro from ESCs are unknown. A thorough comparison of both repertoires should help to validate or invalidate the imprinting status of ESC-derived neural cells.

Here, using RNA-seq and RRBS on F1 hybrid mouse cells and tissues, we show that cortical cells generated from ESCs reflect the in vivo cortex with respect to the parent-of-origin-dependent gene expression and DNA methylation at most imprinted loci. Thus, in vitro corticogenesis should help to identify the function of these well-conserved IGs in corticogenesis as well as the poorly known mechanisms of brain-specific imprinting.

## Material and Methods

### ESC Lines and In Vitro Corticogenesis from Embryonic Stems Cells

E14Tg2a (E14) embryonic stems cells (ESCs) were maintained on gelatin-coated dishes in DMEM (Life Technologies) supplemented with 15% ES-certified FBS (Life Technologies), 0.1 mM nonessential amino acids (Life Technologies), 1 mM sodium pyruvate (Life Technologies), 0.1 mM β-mercaptoethanol (Sigma), 50 U/mL penicillin/streptomycin, and $10^3$ U/mL LIF (Millipore) as previously described (Gaspard et al. 2009). Hybrid BJ1 (♀C57BL/6J × ♂JF1/Ms) F1 and JB6 (♀JF1/Ms × ♂C57BL/6J) F1 ESCs were described in Kota et al. (2014). These cells were maintained on gelatin-coated dishes in ESGRO complete plus medium (Millipore, SF001-500P), which contains LIF, BMP4 (Ying et al. 2003), and a GSK3β inhibitor (Ying et al. 2008). Note that BJ1 corresponds to BJ1 line while JB6 is named JB1 line in Kota et al. (2014).

To generate cortical cells in vitro, E14 ESCs were differentiated as described previously (Gaspard et al. 2009). Hybrid ESCs were differentiated as E14 ESCs, except that they were plated onto matrigel (human ESC qualified matrix, BD)-coated dishes and that DDM was supplemented with B27 (without vitamin A) to improve their survival (Kota et al. 2014). For all lines, DDM medium was supplemented with cyclopamine (1 μM) from day 2 to 10 to enhance dorsalization of telencephalic progenitors as described previously (Gaspard et al. 2009). Differentiation was stopped after 12 or 21 days of culture.

All animal procedures were conducted in accordance with the protocol approved by the Institutional Animal Care and Use Committee.

### Immunofluorescence and Imaging

Immunofluorescence experiments were performed as described in Gaspard et al. (2009). Primary antibodies were incubated overnight at 4 °C and secondary antibodies for 2 h at room temperature. Nuclei were stained with DAPI. Coverslips were mounted with Mowiol. Five to 10 different areas per coverslip were examined with an AxioimagerZ1 fluorescent microscope (Zeiss). The proportions of E14, BJ1, or JB6 cells expressing NESTIN, TUBB3, and GFAP were measured semi-automatically by measuring the proportions of marker-positive areas into the total DAPI-labeled areas on low magnification images, as described by Sun et al. (2013). In more details, the 3 markers were detected with the same Cy3 secondary antibody and total cells were labeled with DAPI. All immunofluorescence data were acquired with the same highly stringent parameters to remove unspecific signal, which may result in underestimation of the % of cells positive

for a given marker, using an imagerZ1 microscope (Zeiss). For each coverslip, 25 images were taken at low magnification (×5) using the Mosaic mode for DAPI and Cy3 (NESTIN, TUBB3, or GFAP). Areas occupied by all the cells ("areaBlue", DAPI) and by the cells expressing the marker of interest ("areaMarkerInBlue", Cy3) were then determined on the reconstituted image (equivalent to 25 images at ×5) using a homemade script in Fiji (available upon request). The percentage of area occupied by the marker in total (DAPI) area was calculated as follows: (areaMarkerInBlue/areaBlue) * 100.0. Data are the average of 3–4 independent differentiations. Antibodies are listed in Supplementary Experimental Procedures.

### RT-qPCR

RT-qPCR was done as described in Al Adhami et al. (2015). Briefly, total RNAs were reverse-transcribed using MMLV-RT and N6 primers (Life Technologies). Quantitative PCR (qPCR) was performed in duplicate or triplicate using SYBR Green Mix (Roche) on a Light Cycler LC480 Real-Time PCR system (Roche) in 384 well plates with 2 ng of equivalent RNA per point of qPCR. The selection of housekeeping genes was performed using geNorm (Vandesompele et al. 2002). The level of expression of each gene X was normalized to the geometric mean of the expression levels of 3 housekeeping genes R (*Gus*, *Tbp*, and *Gapdh*) according to the formula: X/geometric mean (R1, R2, R3) = $2^{-[Cp(X) - \text{arithmetic mean } (Cp(R1),Cp(R2),Cp(R3))]}$, where Cp is the crossing point. Quantitative PCR primers are listed in Supplementary Table 1.

### RNA-seq

Cells and brain tissues were lysed in RNA now and total RNAs were prepared according to the manufacturer's instructions (Ozyme). RNAs were DNAse-treated (Ambion) and their integrity was checked on a 2100 Bioanalyser (Agilent). Strand-specific RNA sequencing was performed at the MGX facility (www.mgx.cnrs.fr) with 3–4 replicates per reciprocal cross of in vivo cortex at embryonic day 13.5 (E13.5) and P0, 2 replicates of undifferentiated BJ1 and JB6 ESCs, BJ1 and JB6 ESCs differentiated into cortex for 12 and 21 days, and 3 replicates of E14 at d12 and d21. Thirty to 50 million high-quality 50 nt single-end reads per sample were generated using Illumina HiSeq 2000 (see Supplementary Table 2). The reads that passed the base caller purity filter (see Supplementary Table 2) were aligned to a hybrid B6/JF1 mRNAs sequence set with IUPAC ambiguous codes at single-nucleotide polymorphisms (SNPs) using Novoalign (Novoutil IUPAC). The B6-JF1 SNPs were downloaded from ftp://molossinus.lab.nig.ac.jp/pub/msmdb/For_Seq_Analysis (Takada et al. 2013). The E14 129P2 reads were aligned against a hybrid B6/129P2 genome where all the B6 bases were replaced with their 129P2 counterparts at all known B6–129P2 SNP positions. The B6–129P2 SNPs were obtained from the Sanger Institute. Counting of different bases at SNP positions was performed using SAMtools/mpileup. The annotation of SNPs was performed using Annovar (Wang et al. 2010).

More details regarding processing and analysis of RNA-seq data can be found in Supplementary Experimental Procedures. The RNA-seq data from this study have been submitted to the NCBI Gene Expression Omnibus (GEO; http://www.ncbi.nlm.nih.gov/geo/) under accession number GSE58523.

### Statistics to Determine Parent-of-Origin-Dependent Expression from RNA-seq Data

We designed a novel statistical method to test for the parent-of-origin-dependent gene expression. This method, called ISoLDE for Integrative Statistics of alleLe Dependent Expression, is a robust nonparametric adaptation of the classical z-test to compare 2 proportions. Robustness was improved through the use of the median absolute deviation as a quantification of expression variability among replicates. This method is extensively described in Supplementary Material (and Reynès et al. in preparation) and available as a Bioconductor package (http://bioconductor.org/packages/ISoLDE/).

### Confirmation of Parent-of-Origin-Dependent Expression by Restriction Fragment Length Polymorphism Analysis and Sanger Sequencing

The measurement of parent-of-origin-dependent expression was essentially performed as described in Kohda et al. (2006). Briefly, genomic DNA and cDNA from ESCs (d0, d12, and d21), dorsal telencephalon (DT and E13.5), and cortex (P0) were PCR-amplified using Taq (NEB) with primers surrounding the polymorphic region. Two techniques were used depending on the nature of the polymorphism: (1) analysis by restriction fragment length polymorphism (RFLP) as for *Meg3* using Bsh1236i, *H19* using BclI, or *Peg3* using TaqI; (2) direct sequencing of the PCR amplicons for *Dlk1*, *Peg10*, *Osbpl15*, *Phactr2*, *Nap1l4*, and *Dhcr7*. PCR products were purified and sequenced by Cogenics. Primer sequences are listed in Supplementary Table 1.

### Reduced Representation Bisulfite Sequencing

Genomic DNAs were prepared using PureLink genomic DNA kit (Life Technologies). Reduced representation bisulfite sequencing (RRBS) was performed on 13 conditions in duplicates: E14 (at d0, d12, and d21), BJ1 (at d0, d12, d21, E13.5, and P0), and JB6 (at d0, d12, d21, E13.5, and P0) as described by Auclair et al. (2014) with slight modifications. Briefly, 200 ng of genomic DNA were digested with *Msp*I (Thermo Scientific) for 5 h, followed by end-repair, A-tailing (with Klenow fragment, Thermo Scientific), and ligation to methylated indexed Illumina adapters using a T4 DNA ligase (Thermo Scientific) in Tango 1× buffer. Fragments were purified using AMPure XP magnetic beads (Agilent) as described in Boyle et al. (2012). Two rounds of bisulfite conversion were then performed using the EpiTect kit (Qiagen). Final RRBS libraries were PCR-amplified with PfuTurbo Cx hotstart DNA polymerase (Agilent) as follows: 95 °C for 2 min, 14 cycles (95 °C for 30 s, 65 °C for 30 s, and 72 °C for 45 s), 72 °C for 7 min. The libraries were purified with AMPure magnetic beads, quantified with a Qubit fluorometer (Life Technologies), and verified by Fragment analyzer (Advanced Analytical) and qPCR (Roche). Directional libraries were sequenced (100 nt single-end reads) on an Illumina HiSeq2000 at MGX facility. Reads were processed and analyzed with tools developed at the Brabaham Institute (Trim_galore, Bismark; (Krueger and Andrews 2011) and Seqmonk). An average of 30 million reads per sample were mapped and bisulfite conversion rate was 99.83 ± 0.09% for the 26 samples (see Supplementary Table 5). Hybrid samples displayed 12–13% informative reads for each genome (C57BL/6 and JF1; not shown). More details are provided in Supplementary Material. RRBS data have been submitted under accession number GSE75485.

### Methylation Analysis by Targeted Bisulfite Sequencing of Specific Loci

DNA extraction was done as previously described (Arnaud et al. 2006) and bisulfite conversion was performed using the EZ DNA methylation™ Gold Kit from Zymo (ref. D5006), according to the manufacturer's instruction. PCR amplifications, cloning, and

sequencing of specific loci were performed as previously described (Arnaud et al. 2006). Primers are listed in Supplementary Table 1.

## Results

### Corticogenesis from Hybrid ESCs

To investigate the parent-of-origin-dependent gene expression and DNA methylation profiles of in vivo and in vitro cortices, we designed an experimental strategy (see Supplementary Fig. 1) that takes advantage of the 12 508 968 strain-specific SNPs identified between the genomes of C57BL/6J—hereafter called B6—and *M. m. molossinus* JF1/Ms—hereafter called JF1—mouse strains (Takada et al. 2013). Reciprocal crosses between B6 and JF1 mice were done to ensure that we measured parental genome-specific differences and not strain biases (Wang and Clark 2014; see Supplementary Fig. 1).

We dissected out dorsal telencephalon (DT), the presumptive cortex, at E13.5 and the cerebral cortex at birth (P0) of BJ1 (B6 mother × JF1 father) and JB6 (JF1 mother × B6 father) hybrids (see Supplementary Fig. 1). In parallel, we took advantage of BJ1 and JB6 ESC lines that we recently characterized (Kota et al. 2014; Maupetit-Mehouas et al. 2016) to generate cortical-like cells in vitro (see Supplementary Fig. 1). We used an established protocol that recapitulates the sequential steps of in vivo corticogenesis, including the progressive generation of dorsal telencephalic progenitors, neurons, and finally glia (Gaspard et al. 2008, 2009). We slightly modified this protocol, initially set up for E14Tg2a ESCs (E14 for short), which are derived from the inbred 129P2 mouse strain, to improve the survival of BJ1 and JB6 hybrid ESC-derived neural progenies [see "Material and Methods" and Kota et al. (2014)]. We focused our study on days 12 (d12) and 21 (d21) of in vitro corticogenesis, because in E14 ESC-derived cells, neural progenitors and neurons form the main cell population at d12 and d21, respectively (Gaspard et al. 2008). Hence, the d12 and d21 cellular compositions grossly resemble those of E13.5 DT and P0 cortex, respectively (Gaspard et al. 2008). The B6 mice that were used to generate BJ1 and JB6 ESC lines carried a *Pou5f1-GFP* transgene that was no longer expressed at d12 and d21 of in vitro corticogenesis, as expected for a pluripotency marker (Fig. 1A). Transcripts for markers of proliferation (*Pcna*) and pluripotency (*Pou5f1* and *Nanog*) decreased during E14 and hybrid ESC-derived corticogenesis (Fig. 1B), in line with the GFP expression pattern (Fig. 1A). In contrast, neural (*Nestin*, *Tubb3*, and *Fabp7*) and cortical (*Pax6*, *Coup-Tf1*, *Emx1*, *Bf1*, and *Otx2*) markers increased in hybrid- as well as in E14-derived cortical cells (Fig. 1B). Immunofluorescence experiments confirmed that neural progenitors (NESTIN+ cells) increased from d0 to d12, and neurons (TUBB3+ cells) (Fig. 1C–E) and glial cells (GFAP+ cells; not shown) increased from d12 to d21 in proportions that were not significantly different between E14 and hybrid cells (Fig. 1C,D). Hybrid neural progenitors (NESTIN+ cells) also expressed the cortical marker PAX6 (Fig. 1E). Furthermore, the hybrid neurons expressed the known markers of cortical layers REELIN, TBR1, CTIP2, and BRN2 at d21 (Fig. 1F). Taken together, these data show that hybrid cells generated the whole cortical lineage and that their progenies resembled those of E14 ESCs, whose cortical potential has been extensively characterized previously (Gaspard et al. 2008).

### Transcriptome-Wide Analysis Shows Similarities Between In Vivo and In Vitro Cortices

Next, we performed strand-specific RNA-seq on BJ1 and JB6 cortices generated either in vivo (at E13.5 and P0) or in vitro (at d12 and d21; see Supplementary Fig. 1 and Table 2). We also performed RNA-seq of undifferentiated BJ1 and JB6 ESCs to measure the dynamics of gene expression during in vitro corticogenesis and of E14-derived in vitro cortices (at d12 and d21) as controls. At least 2 biological replicates for each reciprocal cross were sequenced (see Supplementary Table 2). To estimate how similar to cortical tissue the cells generated in vitro were, we performed clustering of our samples with other neural and nonneural (liver and heart) samples retrieved from the GEO database (see Supplementary Table 2). Biological replicates grouped well together, demonstrating a good reproducibility (Fig. 2A). At both time points of in vitro corticogenesis (d12 and d21), differentiated hybrid ESCs grouped with the E14-derived neural cells (Fig. 2A). Our cortical samples generated either in vivo or in vitro, clustered closer to other neural samples (cortical neurons in culture and in vivo embryonic and neonatal whole brain samples) than to nonneural samples (liver and heart; Fig. 2A). This shows that the identity of hybrid ESC-derived cells was mainly neural and that corticogenesis likely took place as well as in the reference E14 line.

To further define the transcriptomic signature of samples, we searched for Gene Ontology (GO) terms that were statistically enriched among the 400 most highly expressed genes whose expression was induced at least 10-fold when compared with undifferentiated ESCs. As expected, up-regulated genes included the established markers of DT at E13.5 (including *Emx1*, *Otx1*, *Pax6*, *Foxg1*, *Eomes*, *Reln*, and *Tbr1*) and of cortex at P0 (including *Tubb3*, *Gria1*, *Shank1*, *Mef2c*, *Lmo4*, and *Satb2*; not shown). GO-BP (Biological Process) terms such as "neuron differentiation," "forebrain development," "adhesion," "regulation of transcription," and "cell motion" were enriched in vivo (see Supplementary Fig. 2). This confirms previous RNA-seq experiments on developing cortex (Fietz et al. 2012). All these GO-BP terms, including "forebrain development," were also enriched in the in vitro cortices, together with additional terms describing other cell fates such as "vasculature" and "urogenital development" (see Supplementary Fig. 2), which were observed recently in cortex generated from human ESCs as well (van de Leemput et al. 2014).

To confirm that in vitro cortex identity was predominantly neural, we plotted the normalized RNA-seq counts for known markers of ESCs, endoderm, mesoderm, and neural fates—from early progenitor to synaptic markers—in undifferentiated ESCs, hybrid in vitro and in vivo cortices, and E14 in vitro cortex. Embryonic liver and heart data from the GEO database (see Supplementary Table 2) were also included as positive controls for endoderm and mesoderm, respectively. As expected, the ESC markers *Pou5f1*, *Nanog*, *Lin28a*, and *Dnmt3l* were maximal in ESC samples (Fig. 2B). *Sox2*, an ESC marker also expressed in the developing cortex (Bani-Yaghoub et al. 2006), was well expressed in in vivo and in vitro cortices, but was absent from liver and heart (Fig. 2B). In vivo and in vitro hybrid cortices displayed similar overall gene expression patterns and high expression of neural markers (Fig. 2C). However, neural markers were less expressed in in vitro cortex and this was associated with a slight bias toward the endoderm fate, as shown by the higher expression of *Foxa2*, but there was no bias toward the mesoderm fate (Fig. 2D). Forty-eight markers of the developing cortex, including layer markers (Bedogni et al. 2010), were up-regulated during in vitro corticogenesis from hybrid or E14 ESCs, in a pattern overall similar to the in vivo pattern. However, their levels of expression were higher in vivo than in vitro and there were minor discrepancies regarding the dynamic scale that was reduced in vitro for some genes (Fig. 2E).

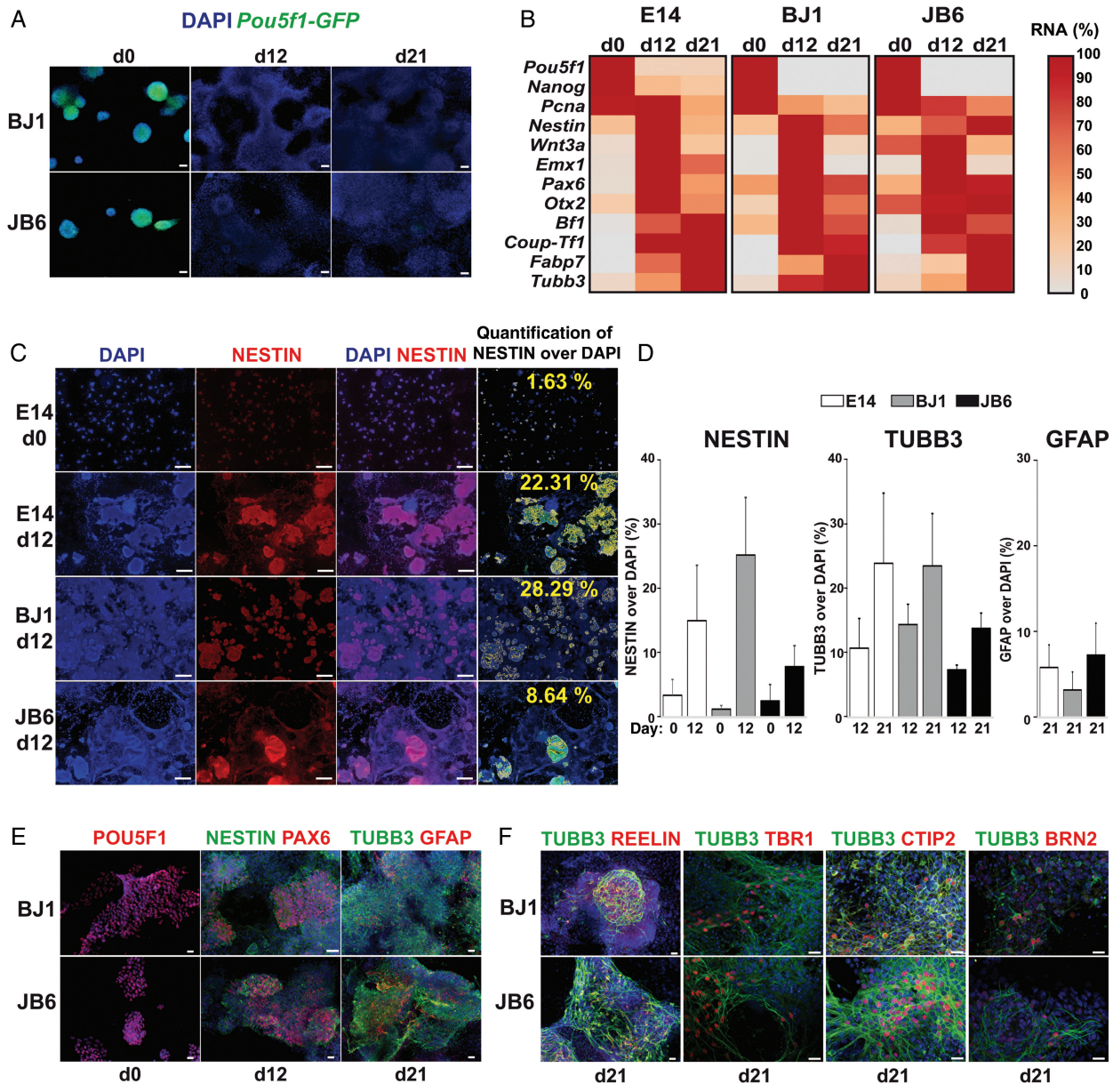


**Figure 1.** Hybrid ESCs generate neural cells with cortical features. BJ1, JB6, and E14 ESCs (d0) were differentiated for 12 (d12) or 21 (d21) days and analyzed by immunofluorescence and RT-qPCR. (*A*) The fluorescence emitted by GFP transcribed from a *Pou5f1-Gfp* transgene decreased during BJ1 and JB6 ESC in vitro corticogenesis. Scale bars: 100 μm. (*B*) Stemness, proliferation, and corticogenesis markers were quantified by RT-qPCR in E14, BJ1, and JB6 at d0, d12, and d21. Data are displayed as a heatmap (gray: minimal expression; dark red: maximum expression for a given gene among d0, d12, and d21) representative of at least 3 independent experiments. (*C* and *D*) Comparison of the corticogenesis potential of hybrid and E14 ESC lines. (*C*) Semi-automatic quantification of the proportion of neural progenitors, neurons, and astrocytes. The proportion of NESTIN+ cells (and TUBB3+ and GFAP+ cells, not shown) was calculated as the % of the Cy3-positive area over the DAPI-labeled area as explained in "Material and Methods." These positive areas are indicated as yellow dots and the obtained values (% of Nestin over DAPI) are shown in the right panels. Scale bars: 500 μm. (*D*) Proportion of NESTIN- (at d0 and d12), TUBB3- (at d12 and d21), and GFAP- (at d21) positive cells in the different cultures by the method described in (*C*). There were no significant differences between BJ1 or JB6 and E14 at any time point, for the 3 markers (Mann–Whitney test, $P > 0.05$). (*E*) BJ1 and JB6 hybrid ESCs expressed the stemness marker POU5F1 at d0. At d12, hybrid NESTIN+ neuronal progenitors expressed PAX6. Neurons (TUBB3+) and glial cells (GFAP+) were present at d21. Scale bars: 20 μm. (*F*) BJ1 and JB6 hybrid cells generated neurons (TUBB3+, green) that expressed markers of various cortical identities shown in red (Cajal-Retzius cells: REELIN; preplate-layer VI: TBR1; layer Vb: CTIP2; layers II/III and Vb: BRN2). Representative pictures of 3 independent cultures are shown. Nuclei were stained with DAPI (blue). Scale bars: 20 μm.

Thus, specific markers and transcriptome-wide signatures showed that hybrid ESCs generated a neural progeny resembling the E14 ESC progeny, which was demonstrated to be fully competent to generate cortical-like cells (Gaspard et al. 2008). Therefore, in vitro differentiation of hybrid ESCs largely reproduced the regulatory programs leading to a cortical-like fate.

## Parent-of-Origin-Dependent Expression of IGs Is Highly Concordant Between In Vivo and In Vitro Cortex

We next investigated whether the parent-of-origin-dependent expression of IGs of in vivo cortex was conserved in vitro. Most of the 140 known IGs investigated here contained several

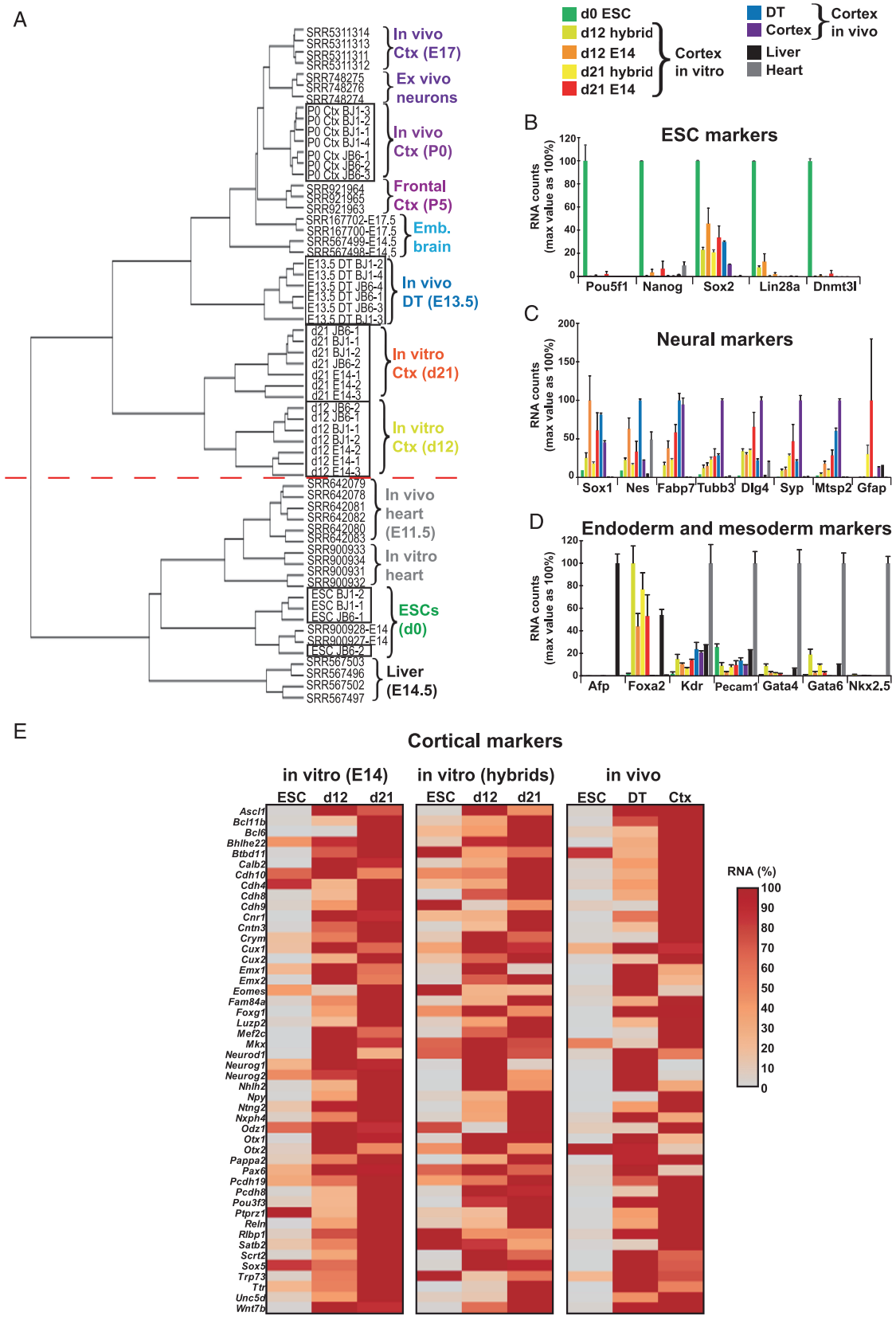


**Figure 2.** Transcriptional identity of ESC-derived cortex is mainly neural. (*A*) Clustering of RNA-seq data obtained in this study (frames) and retrieved from the GEO database: embryonic cortex (E17.5), ex vivo cortical neurons in culture, neonatal frontal cortex (P5), embryonic whole brain (E17.5 and E14.5), embryonic liver and heart, in vitro ESC-derived heart, and E14 ESCs (see Supplementary Table 2). The red dot line separates neural and nonneural samples. (*B–D*) Histograms showing the average of normalized RNA-seq counts + SEM for BJ1–JB6 hybrid ESCs at d0 ($n = 4$), BJ1–JB6 in vitro cortex at d12 ($n = 4$) and d21 ($n = 4$), in vitro cortex from E14 ESCs at

SNPs and only 25, including many miRNAs, had no SNP (see Supplementary Table 3). After removal of the 6 known IGs on the X chromosome, this pinpointed 109 IGs for which the parent-of-origin-dependent expression could potentially be measured. One hundred and seven of these were expressed in both in vivo and in vitro cortices and a majority of these were induced during differentiation (see Supplementary Table 4). Next, RNA-seq reads with B6-JF1-specific SNPs were retrieved to determine the number of maternal and paternal RNA-seq reads (see Supplementary Table 4). Data were analyzed with a novel statistical method that we named ISoLDE for Integrative Statistics of alleLe Dependent Expression (Reynès et al. in preparation). ISoLDE requires replicates of reciprocal crosses and, in contrast to previous methods, positively identifies both genes with parent-of-origin-dependent expression and bi-allelically expressed genes. ISoLDE classifies genes into 5 major categories: maternal, paternal, bi-allelic, filtered out (due to insufficient numbers of reads), and undetermined (UN) when ISolDE cannot affirm they are maternal, paternal, or biallelic. In addition, UN genes showing concordant parental biases in all replicates of both parental crosses are flagged UN-mat or UN-pat.

ISoLDE was first applied to the in vivo samples (E13.5 DT and P0 cortex). Of 109 IGs with at least one B6-JF1 SNP (see Supplementary Table 3), 33 IGs were filtered out and 5 were UN in both stages (Fig. 3 and see Supplementary Table 4). For the remaining 71 IGs, 34 were bi-allelic and 37 showed a significant parent-of-origin-dependent expression at either E13.5 or P0 (Fig. 3 and see Supplementary Table 4). This category includes *Eif2c2*, *A230057D06Rik*, *D7Ertd715e*, *Adam23*, and *Phactr2* that were recently identified as imprinted by others (Wang et al. 2011; DeVeale et al. 2012). Twenty-eight IGs were expressed exclusively from one parental allele (such as *Peg10*, *Peg13*, *Cdkn1c*, *H19*, and *Plagl1*), and 9 IGs (*Adam23*, *Blcap*, *Copg2*, *Asb4*, *Impact*, *Eif2c2*, *Phactr2*, *Trappc9*, and *Ube3a*) were expressed mainly from one parental allele and also weakly from the other allele (see Supplementary Table 4). *Ube3a* was the only IG whose parental bias was significantly different between E13.5 (bi-allelic) and the newborn cortex (preferentially maternal; Fig. 3 and see Supplementary Table 4), as previously reported (Kohama et al. 2012).

We next compared the parent-of-origin-dependent expression of IGs between in vitro and in vivo cortices. To this aim, we calculated a concordance score: for each comparison between in vivo and in vitro cortices at related developmental stages (i.e., d12 vs. E13.5 DT and d21 vs. P0 cortex), we gave a score ranging from 0 for a total discordance to 1 for a perfect match (Fig. 3 and see Supplementary Table 4 and Supplementary Material for details in score calculation). The average concordance score for the 69 IGs whose parent-of-origin-dependent expression could be measured in both types of cortices was high (0.82 ± 0.28). Notably, 41 IGs were fully concordant with a score of 1 (Fig. 3 and see Supplementary Table 4). There was a perfect or high conservation for IGs known to impact on telencephalon development such as *Mest* (paternal; Sansom et al. 2005), *Cdkn1c* (maternal; Mairet-Coello et al. 2012), *Igf2* (UN-pat; Lehtinen et al. 2011), and *Necdin* (paternal; Kuwajima et al. 2006). Only 9 IGs had a concordance score of <0.5 (*Zim1*, *Blcap*, *Gnas*, *Trappc9*, *Ei2f2c2*, *Adam23*, *Slc38a*, *Slc22a3*, *and Zdbf2*). The less concordant IGs, with a score of 0, were *Adam23* and *Zdbf2*, which were paternal in vivo while they were bi-allelic in vitro (Fig. 3 and see Supplementary Table 4). *Igf2r* and *Slc22a3* were maternal in vitro and UN-mat or bi-allelic in vivo (Fig. 3). It was previously shown that *Igf2r* is bi-allelically expressed when the expression of *Airn* non coding RNA is low (Sleutels et al. 2003). Indeed, we found a lower expression of *Airn* in vivo when compared with in vitro (see Supplementary Fig. 3).

Importantly, we confirmed the parent-of-origin-dependent expression of 9 IGs determined by RNA-seq/ISoLDE using 2 alternative and complementary methods, RFLP and Sanger sequencing of PCR products. We confirmed the bi-allelic expression of *Osbpl5* (Fig. 4A), *Nap1l4*, and *Dhcr7* (see Supplementary Fig. 4A,B), the paternal expression of *Peg10*, *Peg3*, and *Dlk1* (Fig. 4B,E and see Supplementary Fig. 4C), and the maternal expression of *Meg3* and *H19* (Fig. 4D and see Supplementary Fig. 4D), both in vivo and in vitro. Sanger sequencing also confirmed the predominant maternal expression of *Phactr2* measured by RNA-seq at E13.5 (Fig. 4C). Thus, we conclude that the allelic expression of IGs was highly conserved in in vitro cortex at d12 and d21 compared with E13.5 and P0 in vivo cortices.

## Faithful Maintenance of DNA Methylation at Imprinted Loci in In Vitro Cortex

Differential DNA methylation at imprinted DMRs, where only one parental allele is methylated, controls the parent-of-origin-dependent expression of IGs (Ferguson-Smith 2011; Kelsey and Feil 2013). RRBS covers most CpG islands and imprinted DMRs at base resolution, and was used to measure the dynamics of DNA methylation in ESC-derived neural cells (Meissner et al. 2008). To assess whether the methylation at imprinted DMRs was faithfully recapitulated in vitro, RRBS was performed on our 13 conditions in duplicates: E14 (at d0, d12, and d21), and BJ1 and JB6 samples (at d0, d12, d21, E13.5, and P0; see Supplementary Table 5).

We compared all conditions using the 1 175 189 CpGs common with all of the 26 samples and that were covered by at least 10 reads (see Supplementary Table 5 and Fig. 5). The median value of CpG methylation was low in vivo (<8%) and in undifferentiated ESCs (<13%), and methylation increased upon ESC differentiation (>30%, Supplementary Table 5) in agreement with a previous report (Meissner et al. 2008). As a control, we checked that the methylation of the promoter and first exon of *Pou5f1* increased during in vitro corticogenesis (see Supplementary Fig. 6) while *Pou5f1* expression decreased (Fig. 1A,B), as reported for this pluripotency gene (Imamura et al. 2006). Methylomes were highly correlated between replicates (see Supplementary Fig. 5B). The samples clustered into 3 main groups: in vitro differentiated cortical cells, in vivo cortex, and ESCs (see Supplementary Fig. 5A). E13.5 DT and P0 cortex samples displayed the typical bimodal distribution of CpG methylation with CpGs being either unmethylated or fully methylated (see Supplementary Fig. 5C). ESC profiles were intermediate with a fraction of

d12 ($n = 3$) and d21 ($n = 3$), BJ1–JB6 hybrid in vivo DT at E13.5 ($n = 6$) and cortex at P0 ($n = 7$), liver at E14.5 ($n = 3$), and heart at E11.5 ($n = 3$). Data are expressed as the % of the maximal number of reads for each gene. (*B*) Differentiated cortical cells do not express ESC markers, except Sox2. (*C*) In vitro and in vivo cortices but not ESCs express neural genes: *Sox1*, *Nes*, and *Fabp7* (neural progenitors); *Tubb3* (neurons); *Dlg4*, *Syp*, and *Mtsp2* (synapse); *Gfap* (glia). (*D*) Most of the markers of nonneural fates, endoderm (*Afp* and *Foxa2*) and mesoderm (*Kdr*, *Pecam1*, *Gata4*, *Gata6*, and *Nkx2.5*), are barely detected in in vitro and in vivo cortices. (*E*) Heatmaps representing the number of normalized RNA-seq reads for 48 cortical markers during in vitro (from either hybrid or E14 ESCs) and in vivo corticogenesis. DT: dorsal telencephalon (E13.5); Ctx: cortex (P0). Most of these markers are induced during both in vitro and in vivo corticogenesis.

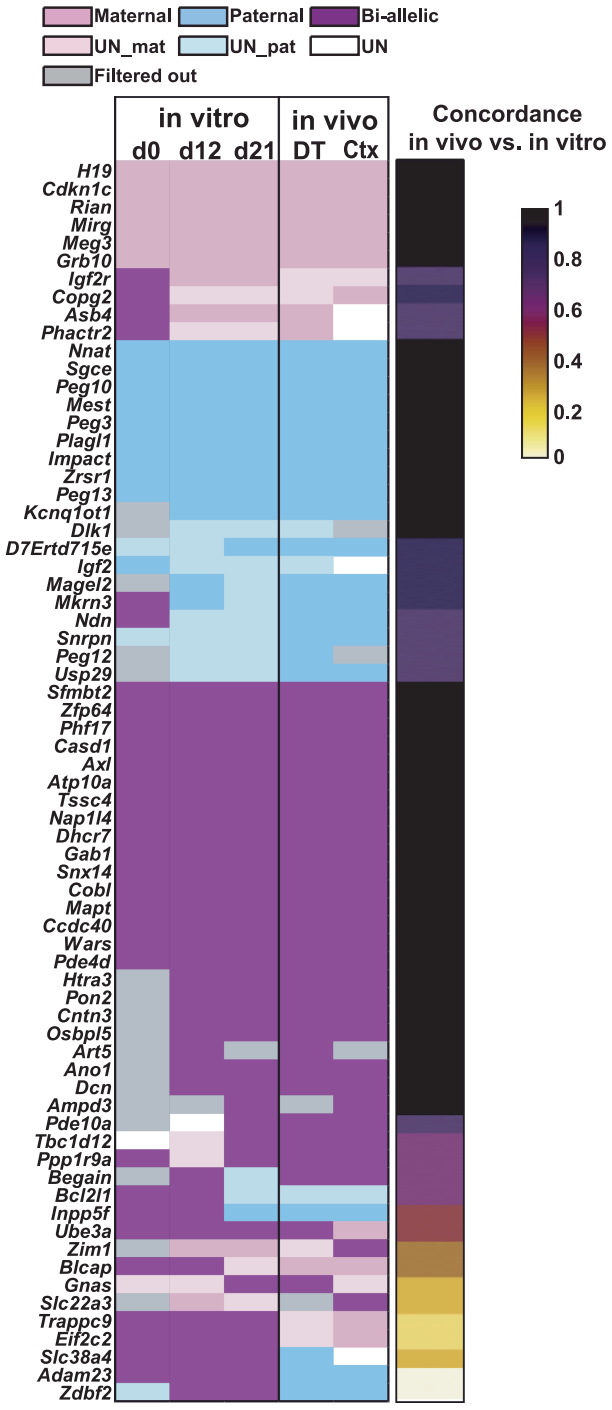


**Figure 3.** The parent-of-origin-dependent expression of IGs is highly concordant between in vivo and in vitro cortices. Statistical analysis of parent-of-origin-dependent expression of IGs was made using ISoLDE on RNA-seq data from hybrid BJ1 and JB6 ESCs (d0), in vitro cortex (d12 and d21), and in vivo cortex (DT at E13.5 and Ctx at P0). IGs were called expressed from the maternal allele (pink), the paternal allele (blue), equally from both parental alleles (i.e. bi-allelic, purple) or undetermined (UN, white). The undetermined genes whose allelic ratios were concordant between all the replicates of both crosses were called UN-mat (light pink) or UN-pat (light blue). The IGs whose parent-of-origin-dependent expression could not be determined because their informative RNA-seq read counts were too low were filtered out (gray). Genes were sorted according to their concordance score between in vivo and in vitro cortices which is color coded in a heatmap from 1: perfect match of parent-of-origin expression between in vivo and in vitro cortices (black) to 0: no concordance (beige). Only the 69 IGs whose parent-of-origin-dependent expression could be measured in both types of cortices are shown.

highly methylated CpGs shifting toward intermediate methylation. JB6 differentiated cells had the same bimodal distribution as the in vivo samples. The methylation profiles of BJ1 differentiated cells (especially at d21) were more like those of d0 ESCs (see Supplementary Fig. 5C). Indeed, d21–BJ1 was less correlated with other samples (see Supplementary Fig. 5B). We used MethylSig (Park et al. 2014) to identify Differentially Methylated CpGs (DMCs) between hybrid ESCs and their progenies to the reference E14 line. BJ1 and JB6 ESCs were very close to E14 ESCs as there was <0.08% of DMCs (with a $q$-value of <0.01 and a difference in methylation >25%; see Supplementary Table 6). JB6 derivatives were close to E14 line (<0.04% of DMCs). BJ1 samples had more DMCs (0.4% at d12 and 10.2% at d21; see Supplementary Table 6), confirming the differences observed in CpG methylation distributions and pairwise correlation matrix (see Supplementary Fig. 5B–C). These data confirmed that the methylome of hybrid ESC-derived cortex resembled that of E14 ESC-derived corticogenesis. Importantly, when comparing in vitro and in vivo hybrid cortices, there were only 7.4% DMCs for d12 versus E13.5 and 8.7% DMCs for d21 versus P0 cortex (see Supplementary Table 6). Methylation was therefore not markedly affected in vitro.

Next, to determine whether methylation at imprinted DMRs was conserved, we compared the methylation of the in vitro differentiated cells with their in vivo counterparts. CpG methylation of 26 known imprinted DMRs (see Supplementary Table 7) was close to 50% (see Supplementary Fig. 7A–E) as expected since one allele should be fully methylated and the other one should be unmethylated. In contrast, 2 DMRs, *Peg12*- and *Gpr1*-DMRs, were respectively hypo- and hypermethylated, but this was not associated with the in vitro culture as it was observed also in vivo (see Supplementary Fig. 7B–E). Finally, only 2 of 26 DMRs showed a high number of DMCs between both d12 and E13.5 DT and d21 and P0 cortex: *Slc38a4*-DMR was hypomethylated and *Zdbf2*-DMR hypermethylated in vitro (see Supplementary Table 6 and Fig. 7B–E). *H19*-DMR was hypermethylated only in d21 cortical cells compared with P0 cortex (see Supplementary Table 6 and Fig. 7B–E) and this was confirmed by COBRA, which also confirmed the proper DNA methylation at *Kcnq1* (KvDMR), *Nnat*-DMR, and *Peg3*-DMR (see Supplementary Fig. 7F). Combined, these data suggest that methylation at imprinted DMRs (without taking into account the parental origin of the methylated allele) was not markedly altered in vitro.

Next, we investigated whether the parental origin of methylation at imprinted DMRs was also conserved. The parental origin of methylation of 7 loci (*Mcts2*, *Gnas1a*, *Peg10*, *Nap1l5*, *Rasgrf1*, *Slc38a4*, and *Igf2r*) could not be determined because there was no B6-JF1 SNPs in the sequenced *MspI* fragments. Consistent with methylation data on both alleles whatever their parental origin, methylation of each parental allele was also well conserved at 14 imprinted DMRs (Fig. 5A–C and see Supplementary Fig. 8). For instance, *Impact*-, *Plagl1*-, and *Kcnq1*-DMRs were methylated only on the maternal chromosome while *Dlk1-Meg3* (IG-DMR), *Meg3*- (or *Gtl2*, promoter), and *Nesp*-DMRs were predominantly methylated on the paternal chromosome in both types of cortex (Fig. 5A–B and see Supplementary Fig. 8). This agrees with previous findings (Ferguson-Smith 2011). Statistical analysis revealed a significant difference in the maternal allele methylation for only 2 DMRs: *H19* and *Zdbf2* (Figs. 5C and see Supplementary Fig. 8 and Table 6), which gained methylation on the maternal chromosome in in vitro cortex (Fig. 5A and see Supplementary Fig. 8). A few CpGs out of all the ones tested CpGs in the *Grb10*- and *Gnas*-DMRs gained paternal methylation in vitro (Fig. 5C and see Supplementary Fig. 8 and Table 6). Parent-of-origin methylation was confirmed by targeted bisulfite sequencing of 2 specific loci: *Nnat* (in vitro

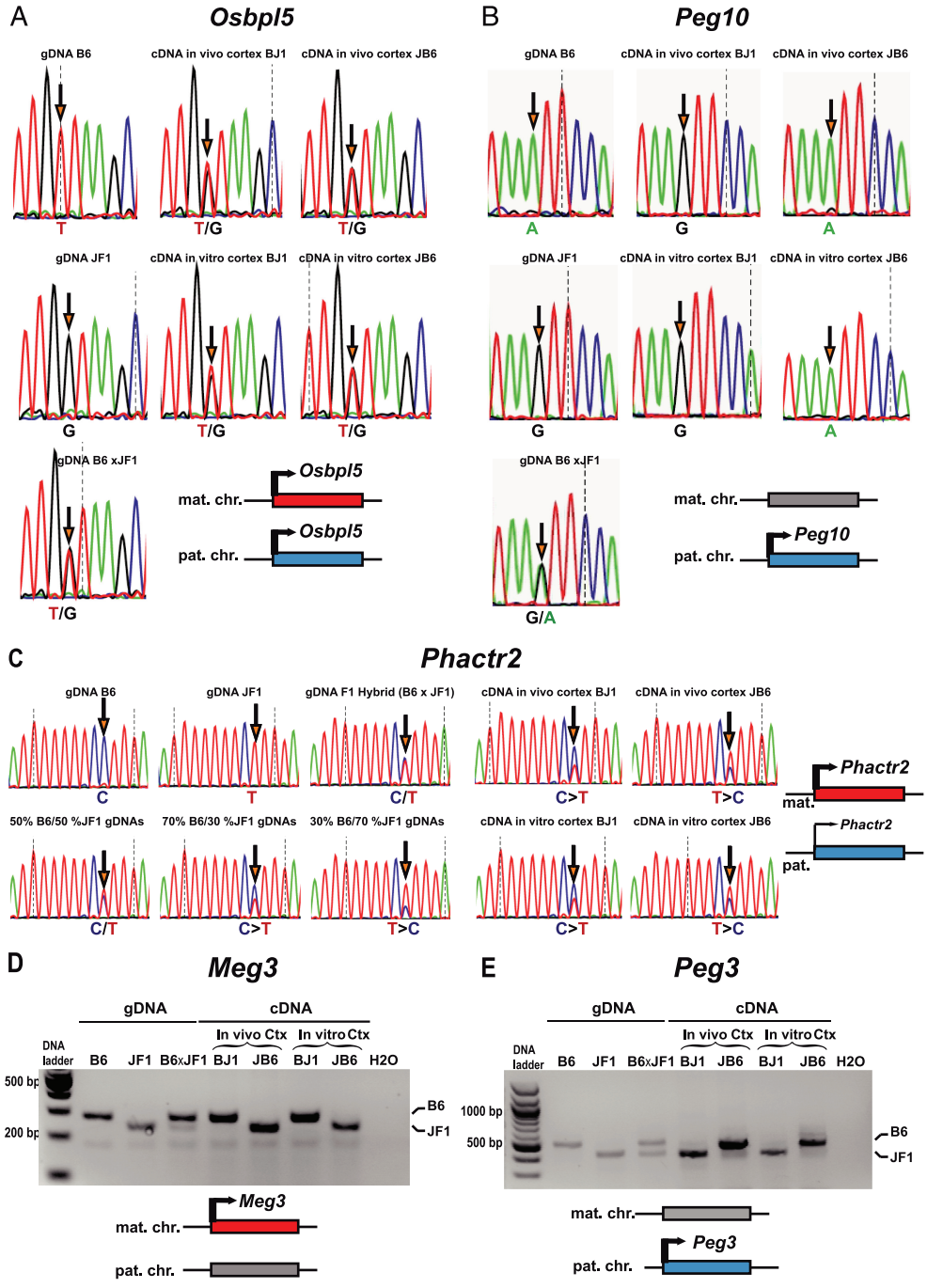


**Figure 4.** Parent-of-origin-dependent expression of IGs is confirmed by Sanger sequencing and RFLPs. The parent-of-origin-dependent expression of one bi-allelically (*Osbpl5*, A), 2 paternally (*Peg10*, *B* and *Peg3*, *E*), and 2 exclusively (*Meg3*, *D*) or preferentially (*Phactr2*, *C*) maternally expressed genes was confirmed. B6, JF1, and BJ1 genomic DNAs and hybrid cDNAs were PCR-amplified from in vivo E13.5 DT and in vitro d12 cortex for all genes, except *Meg3* which was amplified from in vivo P0 cortex and in vitro d21 cortex. (*A*–*C*) Sanger sequencing of PCR products. For *Phactr2* only (*C*), different ratios of B6 and JF1 gDNAs were used to ensure that Sanger sequencing could reveal subtle differences in allelic expression. Orange arrows indicate the SNP positions. Representative chromatograms from $n = 2$–3 independent experiments are shown. (*D* and *E*) RFLPs. PCR products were digested with Bsh1236i (*Meg3*, *D*) or *TaqI* (*Peg3*, *E*) and run into BET-stained agarose gel (2%). 100 bp ladder (NEB) and negative PCR control (water) are shown. Representative gel pictures from 3 independent experiments are shown. Drawings illustrate the interpretation of the data with the expressed allele colored in red (maternal) or blue (paternal) and the inactive parental allele in gray.

methylation similar to in vivo) and *Zdbf2* (hypermethylation of the maternal allele in vitro when compared with in vivo; Fig. 5*D*–*F*).

From the combined data, we conclude that both parent-of-origin-dependent gene expression and methylation of in vivo cortex are largely reproduced by in vitro cortex. Figure 6 shows examples of discordance (*Gpr1-Zbdf2* and *H19-Igf2* loci) and of concordance (*Kcnq1*, *Peg3*, and *Dlk1-Dio3* loci) in the imprinting status between in vitro and in vivo cortices.

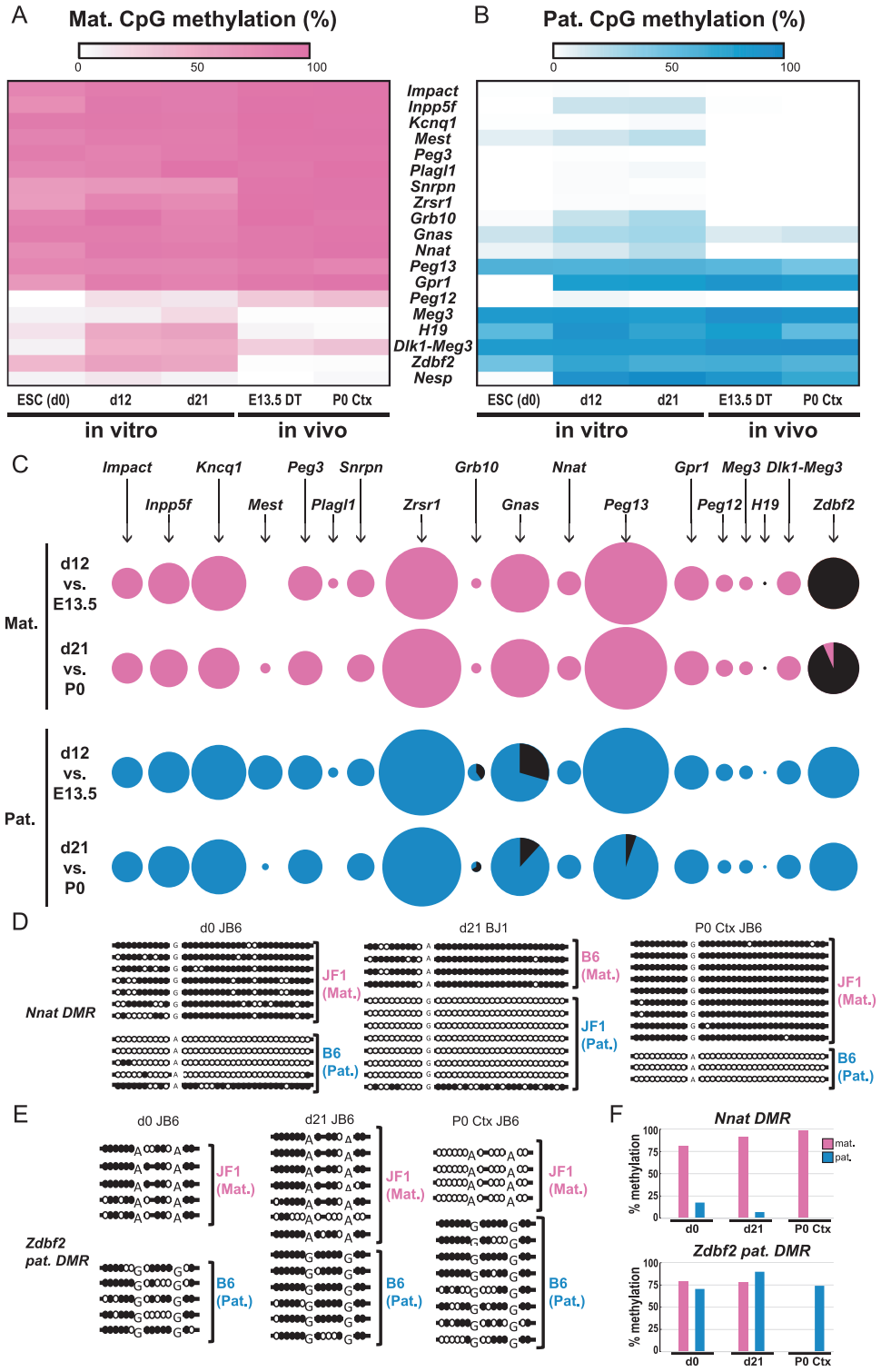


**Figure 5.** Parental allele CpG methylation at imprinted DMRs is well reproduced by in vitro corticogenesis. (*A* and *B*) Heatmap representation of the methylation levels obtained by RRBS for 19 imprinted DMRs on maternal (*A*) and paternal (*B*) chromosomes performed on BJ1 and JB6 at d0, d12, d21, E13.5, and P0. Values are the means of the % of methylation in all CpGs present in each DMR in the 4 hybrid samples. (*C*) Sparkline representation of statistical analysis of differential methylation between d12 versus E13.5 and d21 versus P0 cortices on maternal and paternal chromosomes measured by RRBS. Data are represented as circles whose surface reflects the total number of CpGs tested for each of the 18 DMRs (values are indicated in Supplementary Table 6). Differentially methylated cytosines between d12 versus E13.5 and d21 versus P0 are indicated as black sectors, whereas cytosines whose methylation are conserved are colored in pink and blue for maternal and paternal chromosomes, respectively. For example, the entirely blue and pink circles at *Impact* DMR show that parent-of-origin-dependent methylation was conserved for the 9 CpGs measured at *Impact* DMR on both parental chromosomes, whereas the entirely black circle for d12 versus E13.5 at *Zdbf2* maternal DMR indicates 15 DMCs out of 15 tested CpGs and therefore no conservation of maternal CpG methylation at *Zdbf2*-DMR. DMCs in *Nesp* DMR could not be tested because its CpGs were covered by <10 informative reads. (*D*–*F*) Methylation pattern at 2 imprinted loci was confirmed by bisulfite sequencing. Bisulfite-treated genomic DNAs from BJ1 or JB6 in vitro (ESC d0 and d21) and in vivo (P0 Cortex) samples were PCR-amplified at the indicated loci (*D*, *Nnat*-DMR; *E*, *Zdbf2*-DMR), subcloned, and sequenced. Filled and open circles denote methylated and unmethylated CpGs, respectively. The percentage of CpG methylation is shown in *F*.

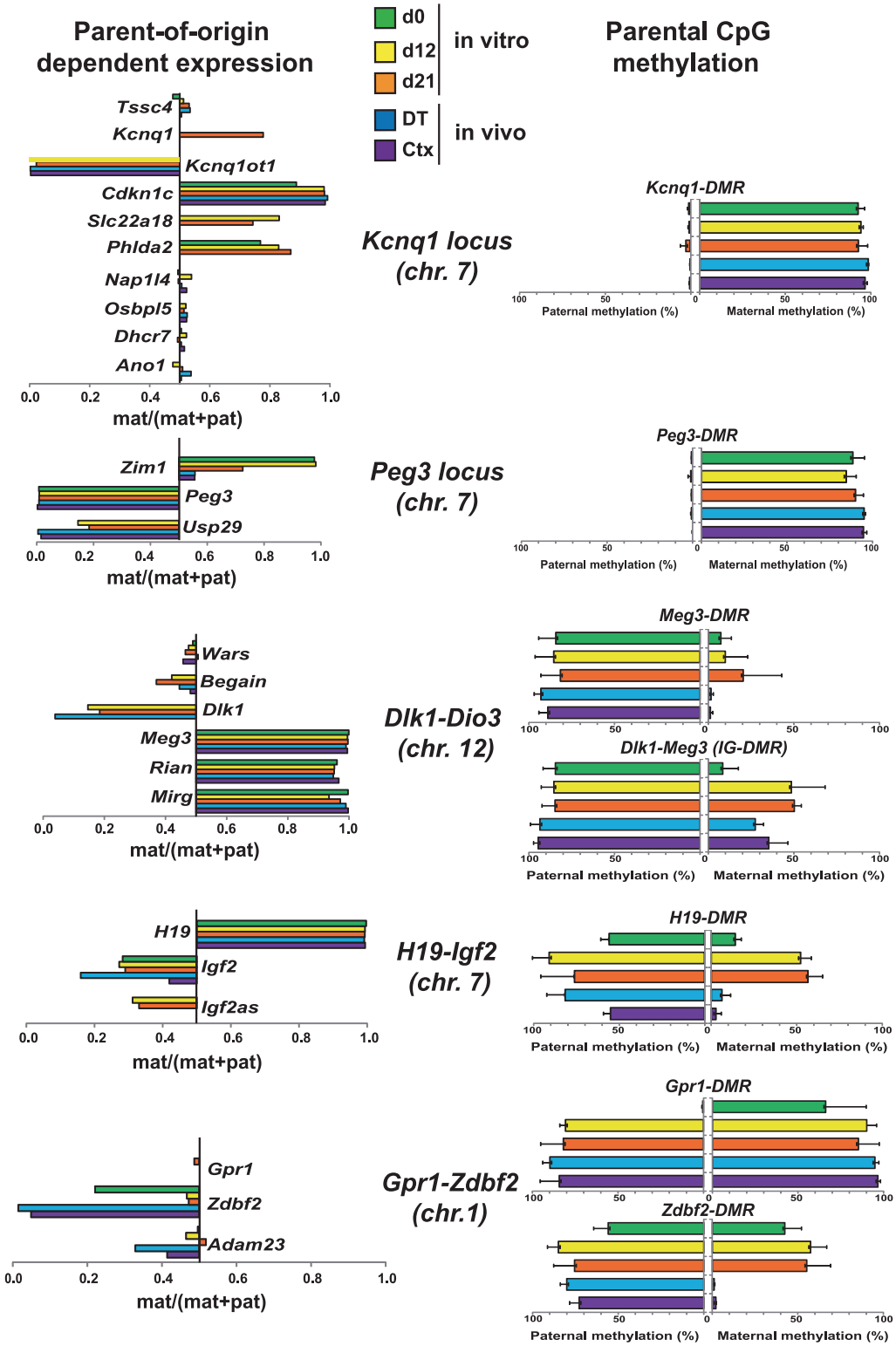


**Figure 6.** Summary of parent-of-origin-dependent gene expression and DNA methylation at 5 representative imprinted loci. The average maternal expression ratio (mat/(mat + pat)) was plotted for genes belonging to 5 imprinted loci in ESC (d0), in vitro cortex (d12 and d21), and in vivo cortex (E13.5 DT and P0 cortex) (left panels). *Usp29* (d0), *Zim1* (d0), *Igf2as* (d0, E13.5, and P0), *Ano1* (d0), *Osbpl5* (d0), *Phlda2* (E13.5 and P0), *Slc22a18* (d0, E13.5, and P0), *Kcnq1ot1* (d0), *Kcnq1* (d0, d12, E13.5, and P0), *Dlk1* (d0 and P0), *Begain* (d0), *Airn* (d0, d12, E13.5, and P0), *Slc22a3* (d0 and E13.5), and *Gpr1* (d0, d12, E13.5, and P0) were filtered out in the samples indicated in parentheses and are thus not represented. The right panels depict the percentage of CpG methylated on the paternal and maternal alleles (mean + SD of 4 hybrid samples) at the corresponding DMRs obtained by RRBS. Note the well-conserved imprinted status in in vitro cortex at *Peg3*, *Kcnq1*, and *Dlk1-Dio3* loci while methylation only, or both methylation and allelic expression, are affected in vitro at *H19-Igf2* or *Gpr1-Zdbf2* loci.

## Discussion

The ability to steer the differentiation of pluripotent stem cells toward cortical cell types in vitro is instrumental in generating accurate alternative models of corticogenesis and in producing cortical cells for regenerative medicine. However, this approach is potentially limited by epigenetic variability and instability triggered by cell culture, notably in ESCs (Rugg-Gunn et al. 2007; Cahan and Daley 2013; Ma et al. 2014). Until now, the epigenetic status of ESC-derived cortex was unknown. In the present report, we focused on IGs because (1) several IGs are involved in brain development and function (Wilkinson et al. 2007; Plasschaert and Bartolomei 2015), (2) imprinted loci are exquisitely sensitive to alteration of their epigenetic status (Adalsteinsson and Ferguson-Smith 2014), and (3) dysregulation of imprinting, which can occur during in vitro culture (Greenberg and Bourc'his 2015), is sufficient to trigger carcinogenesis (Holm et al. 2005). Parent-of-origin-dependent transcription of IGs is the functional output of epigenetic modifications, notably DNA methylation, at imprinted loci (Adalsteinsson and Ferguson-Smith 2014). Therefore, DNA methylation and transcription can be combined to estimate imprinting status. One technical advantage of evaluating imprinting by RNA-seq and RRBS over ChIP-seq targeted at histone modifications is that these 2 approaches do not rely on antibodies that frequently show difficulties in detecting their intended targets (Rothbart et al. 2015). We have studied parental genomic imprinting on hybrid in vivo and in vitro cortices at both epigenomic and transcriptomic levels. We conclude that in vitro corticogenesis maintains parent-of-origin-dependent expression and DNA methylation at most imprinted loci.

The brain is a recognized hotspot for imprinting, but the identity of IGs showing parent-of-origin-dependent expression specifically in the cortex was unknown. We report that 34 IGs are bi-allelically expressed and 37 IGs have a parent-of-origin-dependent expression in the in vivo developing mouse cortex. These numbers are consistent with previous transcriptome-wide studies using RNA-seq on F1 hybrid embryos (Babak et al. 2008), whole brain (Wang et al. 2008; DeVeale et al. 2012), placenta (Wang et al. 2011), and mouse embryonic fibroblasts (Tran et al. 2014; see Supplementary Table 4). We did not identify any new IG. If new IGs were to be found, they would probably have to be searched for in a defined cortical subtype and at a precise corticogenesis stage. We could not measure the allelic expression of *Gatm*, *Kcnk9*, *H13*, *Mcts2*, and *Qpct* because they had no exonic B6-JF1 SNP. Using hybrid crosses from different strains could increase the repertoire of parent-of-origin-dependent gene expression, including possibly new ones. In addition, the expression of certain IGs was fully monoallelic while other IGs were also weakly expressed from the normally repressed allele. This partial or "noncanonic" (Bonthuis et al. 2015) parent-of-origin-dependent expression (Prickett and Oakey 2012) could be the result of incomplete silencing or partial de-repression of the normally silent allele, as observed for *Dlk1* in neural stem cells (Ferron et al. 2011). Another possibility is that our samples were heterogeneous and composed of cells where the parent-of-origin-dependent expression was absolute for a given IG, surrounded by cells where the same IG was bi-allelically expressed. For example, *Igf2* is known to be bi-allelically expressed in the choroid plexus and meninges at P0 (Charalambous et al. 2004) and strictly paternally expressed in other neural cell types. The heterogeneity of our in vivo P0 cortex samples could then explain the 40% maternal–60% paternal *Igf2* expression. Isolation of pure population of cells and single cell RNA-seq could determine whether all cells exhibit the same parent-of-origin-dependent expression of IGs.

We quantified CpG methylation by RRBS and compared both parent-of-origin-dependent expression and DNA methylation at imprinted loci between in vivo and in vitro cortices. So far, few in vitro models have reproduced the in vivo parent-of-origin-dependent expression of IGs. The available examples include only one IG at a time: *Ube3a* (Kohama et al. 2012), *Igf2r* (Latos et al. 2009), and *Grb10* (Plasschaert and Bartolomei 2015). Here, we faithfully reproduced the parent-of-origin-dependent expression of 41 IGs, whether there were maternally, paternally, or bi-allelically expressed. Notably, some IGs that were bi-allelic in ESCs (*Phactr2*, *Innp5f*, *Asb4*, *Mkrn3*, and *Ndn*) switched to the monoallelic expression observed in vivo. Our in vitro differentiation system also faithfully reproduced cell type-specific mechanisms, as shown for *Grb10*. *Grb10* has a unique tissue-specific imprinting: at E14.5, expression from the paternal allele is predominant in the spinal cord while *Grb10* is maternally expressed in the cortex (Garfield et al. 2011). Our data show that *Grb10* expression is strictly maternal in undifferentiated ESCs and remains so after 12 and 21 days of in vitro corticogenesis, hence mimicking the maternal expression in E13.5 DT and P0 cortex. Our corticogenesis model displaying maternal *Grb10* expression is complementary to that of Plasschaert and Bartolomei (2015), who recently reproduced the paternal expression of *Grb10* in the spinal cord using ESC-derived motoneurons. *Ube3a* did not switch from bi-allelic to maternal during in vitro corticogenesis, as it did in vivo, where its maternal expression increased from 52% at E13.5 to 63% at P0 without any change in the *Snrpn*-DMR methylation. Our hypothesis is that there is less *Ube3a-ATS* in vitro than in vivo because there are less neurons in vitro (see neuronal markers in Fig. 2C). *Zdbf2* and *Adam23* were the 2 most discordant IGs: bi-allelic in vitro and strictly paternal in vivo, as previously reported for *Zdbf2* in ESC-derived neural cells and brain, respectively (Duffie et al. 2014). These aberrant parent-of-origin expressions were associated with, and could be due to the aberrant hypermethylation of the maternal allele of *Zdbf2*-DMR, as observed in some Beckwith-Wiedemann Syndrome patients (Maeda et al. 2014). The aberrant bi-allelic expression of *Slc38a4* in vitro was associated with a global loss of methylation at its DMR located in the promoter of this gene. Unfortunately, the allelic methylation status of this locus could not be determined because it has no SNP. Some changes in DNA methylation were not associated with those in allelic gene expression: the *H19* maternal allele was hypermethylated in vitro, but the allelic expressions of *H19* and *Igf2* were identical in vitro and in vivo. Reciprocally, some changes in parent-of-origin expression could not be linked to those in DNA methylation. *Slc22a3* and *Igf2r* were maternal in vitro but expressed from both parental alleles in vivo, without any detectable change in global DNA methylation at the *Igf2r*-DMR. Allelic expression at this locus is known to be regulated by *Airn*, an anti-sense RNA whose expression is required for the silencing of the paternal alleles (Sleutels et al. 2003). The higher *Airn* expression observed in vitro (see Supplementary Fig. 3) could thus explain that the paternal alleles of *Slc22a3* and *Igf2r* were more repressed in vitro than in vivo. Since we observed several differences at imprinted loci where non coding RNAs are crucial (*Ube3a-ATS* at *Ube3a* locus, *Airn* at *Igf2r* locus, and *Liz* at *Zdbf2* locus), it will be important to understand why these non coding RNAs could be affected in vitro. Besides DNA methylation, other epigenetic features are important for parental genomic imprinting. Recently, it was found that some histone modifications correlate with IG regulation in hybrid ESCs and tissues (Maupetit-Mehouas et al. 2016) but the repertoire of these histone marks in cortex generated from ESCs is unknown. Measuring CpG hydroxymethylation, which is prevalent

in the brain (Kinney et al. 2011), and whose levels drop during adaptation of mouse embryonic fibroblasts to cell culture (Nestor et al. 2015), will also be of interest.

The observed differences between in vitro and in vivo corticogenesis could be linked to differences in cell composition. It is possible that the different cortical cell types were correctly generated, but in proportions different from those observed in vivo. Indeed, cortical neurons of upper layers are known to be underrepresented upon differentiation in vitro (Gaspard et al. 2008; Hansen et al. 2011). The proportion of neurons might be increased by supplementing the corticogenesis media with valproic acid, a histone deacetylase inhibitor that was recently found to increase the number of upper layer neurons in in vitro cortex (Juliandi et al. 2012). In addition, systems that allow 3D cortex generation in vitro should better reflect the cytoarchitecture and organization (and likely epigenetics) of the in vivo cortex (Eiraku et al. 2008; Mariani et al. 2012), although such systems have also their limitations (Lancaster and Knoblich 2014).

Finally, as gene expression and DNA methylation were affected at only a limited number of imprinted loci upon in vitro corticogenesis, our data suggest that some epigenetic mechanisms were largely preserved in vitro. Certainly, imprinting is only one component of the epigenome and other features would need to be studied as well. Given the reported negative impact of prolonged cell culture on epigenetic marks, it would be particularly interesting to extend our findings to human ESCs. The period of time in culture to generate forebrain glutamatergic neurons (Espuny-Camacho et al. 2013) and GABAergic interneurons (Nicholas et al. 2013) from human ESCs is lengthened by several months compared with mice. Furthermore, the repertoire of genes with parent-of-origin-dependent expression in human cortex is only partially known and may be different from the mouse repertoire. Indeed, genes thought to be important for human cortical development, such as *FOXG1*, *OTX1*, and *P73*, are predicted to be imprinted in humans (Luedi et al. 2007), while we found that they are bi-allelically expressed in the mouse cortex (not shown). Epigenomic data obtained from dorsolateral prefrontal cortex and cortical neurospheres derived from human ESCs and recently released by the Roadmap Epigenomics Consortium (Roadmap Epigenomics et al. 2015) could be mined to get insights into the epigenetic signature of in vitro human cortex.

In conclusion, corticogenesis from mouse ESCs displays an established repertoire of parent-of-origin expression and DNA methylation of imprinted loci. This model could be used reliably to unravel the molecular mechanisms involved in selecting the expressed parental allele(s) in the context of imprinting during cortical development. Our findings also provide encouragement to use ESCs to model cortical development and for drug screening. The in vitro corticogenesis system could be a powerful tool to pinpoint drugs that de-repress the silenced parental allele in certain brain diseases associated with perturbed IG expression (Huang et al. 2011) or to estimate the impact of ecotoxic compounds on the epigenetic signatures and the development of cortical cells.

## Authors' Contribution

T.B., C.R., S.K., R.F., P.A., L.J., and A.V. conceived and designed the experiments; T.B., C.R., S.K., S.M.-M., M.P., A.L.D., S.N., P.C., C.Me., C.Ma., and A.V. performed the experiments; T.B., E.D., C.R., S.R., S.M.-M., V.D., R.S., P.A., L.J., and A.V. analyzed the data; T.B., L.J., and A.V. wrote the paper. All authors commented on the manuscript. RNA-seq (GSE58523) and RRBS (75485) data have been deposited in the Gene Expression Omnibus (GEO) database combined in a Superseries (GSE75486).

## Supplementary Material

Supplementary material can be found at http://www.cercor.oxfordjournals.org/online.

## Notes

We thank Ira Espuny-Camacho, Luca Tiberi, and Pierre Vanderhaeghen for advice on in vitro corticogenesis and for critical reading of the manuscript, Tomas Babak for advice on the analysis of the parent-of-origin-dependent gene expression using RNA-seq, Michael Weber, Felix Krueger, and Hala Al Adhami for advice on RRBS, Thomas Keane and David Adams (Sanger Institute) for providing the 129P2 genome sequence, Sandra Acosta for *Emx1* primers sequences, Atsuo Ogura for providing his RFLP protocol, and the Jackson Laboratory for pictures of C57BL/6 and JF1 mice. We thank Maurine Bonabaud, Samia Guendouz, Hugues Parinello, Claire Prevost, Marine Rohmer, and Dany Severac for technical assistance and discussion. We thank William Ritchie for reading our manuscript, Chrystel Lafont for assistance with the ImagerZ1 microscope, and Volker Baecker for the Fiji script. This work was funded by the ANR grants "Epinet", "Bivandev," and "Imprint-RNA". *Conflict of Interest*: None declared.

## References

Adalsteinsson BT, Ferguson-Smith AC. 2014. Epigenetic control of the genome-lessons from genomic imprinting. Genes (Basel). 5:635–655.

Al Adhami H, Evano B, Le Digarcher A, Gueydan C, Dubois E, Parrinello H, Dantec C, Bouschet T, Varrault A, Journot L. 2015. A systems-level approach to parental genomic imprinting: the imprinted gene network includes extracellular matrix genes and regulates cell cycle exit and differentiation. Genome Res. 25:353–367.

Albrecht U, Sutcliffe JS, Cattanach BM, Beechey CV, Armstrong D, Eichele G, Beaudet AL. 1997. Imprinted expression of the murine Angelman syndrome gene, Ube3a, in hippocampal and Purkinje neurons. Nat Genet. 17:75–78.

Arnaud P, Hata K, Kaneda M, Li E, Sasaki H, Feil R, Kelsey G. 2006. Stochastic imprinting in the progeny of Dnmt3L$^{-/-}$ females. Hum Mol Genet. 15:589–598.

Auclair G, Guibert S, Bender A, Weber M. 2014. Ontogeny of CpG island methylation and specificity of DNMT3 methyltransferases during embryonic development in the mouse. Genome Biol. 15:545.

Babak T, Deveale B, Armour C, Raymond C, Cleary MA, van der Kooy D, Johnson JM, Lim LP. 2008. Global survey of genomic imprinting by transcriptome sequencing. Curr Biol. 18:1735–1741.

Babak T, DeVeale B, Tsang EK, Zhou Y, Li X, Smith KS, Kukurba KR, Zhang R, Li JB, van der Kooy D, et al. 2015. Genetic conflict reflected in tissue-specific maps of genomic imprinting in human and mouse. Nat Genet. 47:544–549.

Bani-Yaghoub M, Tremblay RG, Lei JX, Zhang D, Zurakowski B, Sandhu JK, Smith B, Ribecco-Lutkiewicz M, Kennedy J, Walker PR, et al. 2006. Role of Sox2 in the development of the mouse neocortex. Dev Biol. 295:52–66.

Bedogni F, Hodge RD, Elsen GE, Nelson BR, Daza RA, Beyer RP, Bammler TK, Rubenstein JL, Hevner RF. 2010. Tbr1 regulates

regional and laminar identity of postmitotic neurons in developing neocortex. Proc Natl Acad Sci USA. 107:13129–13134.
Bhardwaj RD, Curtis MA, Spalding KL, Buchholz BA, Fink D, Bjork-Eriksson T, Nordborg C, Gage FH, Druid H, Eriksson PS, et al. 2006. Neocortical neurogenesis in humans is restricted to development. Proc Natl Acad Sci USA. 103:12564–12568.
Bonthuis PJ, Huang WC, Stacher Horndli CN, Ferris E, Cheng T, Gregg C. 2015. Noncanonical genomic imprinting effects in offspring. Cell Rep. 12:979–991.
Boyle P, Clement K, Gu H, Smith ZD, Ziller M, Fostel JL, Holmes L, Meldrim J, Kelley F, Gnirke A, et al. 2012. Gel-free multiplexed reduced representation bisulfite sequencing for large-scale DNA methylation profiling. Genome Biol. 13:R92.
Cahan P, Daley GQ. 2013. Origins and implications of pluripotent stem cell variability and heterogeneity. Nat Rev Mol Cell Biol. 14:357–368.
Chamberlain SJ, Lalande M. 2010. Angelman syndrome, a genomic imprinting disorder of the brain. J Neurosci. 30:9958–9963.
Charalambous M, Menheniott TR, Bennett WR, Kelly SM, Dell G, Dandolo L, Ward A. 2004. An enhancer element at the Igf2/H19 locus drives gene expression in both imprinted and non-imprinted tissues. Dev Biol. 271:488–497.
Dean W, Bowden L, Aitchison A, Klose J, Moore T, Meneses JJ, Reik W, Feil R. 1998. Altered imprinted gene methylation and expression in completely ES cell-derived mouse fetuses: association with aberrant phenotypes. Development. 125:2273–2282.
DeVeale B, van der Kooy D, Babak T. 2012. Critical evaluation of imprinted gene expression by RNA-Seq: a new perspective. PLoS Genet. 8:e1002600.
Duffie R, Ajjan S, Greenberg MV, Zamudio N, Escamilla del Arenal M, Iranzo J, Okamoto I, Barbaux S, Fauque P, Bourc'his D. 2014. The Gpr1/Zdbf2 locus provides new paradigms for transient and dynamic genomic imprinting in mammals. Genes Dev. 28:463–478.
Ehninger D, Kempermann G. 2003. Regional effects of wheel running and environmental enrichment on cell genesis and microglia proliferation in the adult murine neocortex. Cereb Cortex. 13:845–851.
Eiraku M, Watanabe K, Matsuo-Takasaki M, Kawada M, Yonemura S, Matsumura M, Wataya T, Nishiyama A, Muguruma K, Sasai Y. 2008. Self-organized formation of polarized cortical tissues from ESCs and its active manipulation by extrinsic signals. Cell Stem Cell. 3:519–532.
Espuny-Camacho I, Michelsen KA, Gall D, Linaro D, Hasche A, Bonnefont J, Bali C, Orduz D, Bilheu A, Herpoel A, et al. 2013. Pyramidal neurons derived from human pluripotent stem cells integrate efficiently into mouse brain circuits in vivo. Neuron. 77:440–456.
Ferguson-Smith AC. 2011. Genomic imprinting: the emergence of an epigenetic paradigm. Nat Rev Genet. 12:565–575.
Ferron SR, Charalambous M, Radford E, McEwen K, Wildner H, Hind E, Morante-Redolat JM, Laborda J, Guillemot F, Bauer SR, et al. 2011. Postnatal loss of Dlk1 imprinting in stem cells and niche astrocytes regulates neurogenesis. Nature. 475:381–385.
Ficz G, Hore TA, Santos F, Lee HJ, Dean W, Arand J, Krueger F, Oxley D, Paul YL, Walter J, et al. 2013. FGF signaling inhibition in ESCs drives rapid genome-wide demethylation to the epigenetic ground state of pluripotency. Cell Stem Cell. 13:351–359.
Fietz SA, Lachmann R, Brandl H, Kircher M, Samusik N, Schroder R, Lakshmanaperumal N, Henry I, Vogt J, Riehn A, et al. 2012. Transcriptomes of germinal zones of human and mouse fetal neocortex suggest a role of extracellular matrix in progenitor self-renewal. Proc Natl Acad Sci USA. 109:11836–11841.
Garfield AS, Cowley M, Smith FM, Moorwood K, Stewart-Cox JE, Gilroy K, Baker S, Xia J, Dalley JW, Hurst LD, et al. 2011. Distinct physiological and behavioural functions for parental alleles of imprinted Grb10. Nature. 469:534–538.
Gaspard N, Bouschet T, Herpoel A, Naeije G, van den Ameele J, Vanderhaeghen P. 2009. Generation of cortical neurons from mouse embryonic stem cells. Nat Protoc. 4:1454–1463.
Gaspard N, Bouschet T, Hourez R, Dimidschstein J, Naeije G, van den Ameele J, Espuny-Camacho I, Herpoel A, Passante L, Schiffmann SN, et al. 2008. An intrinsic mechanism of corticogenesis from embryonic stem cells. Nature. 455:351–357.
Greenberg MV, Bourc'his D. 2015. Cultural relativism: maintenance of genomic imprints in pluripotent stem cell culture systems. Curr Opin Genet Dev. 31:42–49.
Hansen DV, Rubenstein JL, Kriegstein AR. 2011. Deriving excitatory neurons of the neocortex from pluripotent stem cells. Neuron. 70:645–660.
Hirabayashi Y, Suzki N, Tsuboi M, Endo TA, Toyoda T, Shinga J, Koseki H, Vidal M, Gotoh Y. 2009. Polycomb limits the neurogenic competence of neural precursor cells to promote astrogenic fate transition. Neuron. 63:600–613.
Holm TM, Jackson-Grusby L, Brambrink T, Yamada Y, Rideout WM III, Jaenisch R. 2005. Global loss of imprinting leads to widespread tumorigenesis in adult mice. Cancer Cell. 8:275–285.
Huang HS, Allen JA, Mabb AM, King IF, Miriyala J, Taylor-Blake B, Sciaky N, Dutton JW, Lee HM, Chen X, et al. 2011. Topoisomerase inhibitors unsilence the dormant allele of Ube3a in neurons. Nature. 481:185–189.
Imamura M, Miura K, Iwabuchi K, Ichisaka T, Nakagawa M, Lee J, Kanatsu-Shinohara M, Shinohara T, Yamanaka S. 2006. Transcriptional repression and DNA hypermethylation of a small set of ES cell marker genes in male germline stem cells. BMC Dev Biol. 6:34.
Jakovcevski M, Akbarian S. 2012. Epigenetic mechanisms in neurological disease. Nat Med. 18:1194–1204.
Juliandi B, Abematsu M, Sanosaka T, Tsujimura K, Smith A, Nakashima K. 2012. Induction of superficial cortical layer neurons from mouse embryonic stem cells by valproic acid. Neurosci Res. 72:23–31.
Kelsey G, Feil R. 2013. New insights into establishment and maintenance of DNA methylation imprints in mammals. Philos Trans R Soc Lond B Biol Sci. 368:20110336.
Kinney SM, Chin HG, Vaisvila R, Bitinaite J, Zheng Y, Esteve PO, Feng S, Stroud H, Jacobsen SE, Pradhan S. 2011. Tissue-specific distribution and dynamic changes of 5-hydroxymethylcytosine in mammalian genomes. J Biol Chem. 286:24685–24693.
Kohama C, Kato H, Numata K, Hirose M, Takemasa T, Ogura A, Kiyosawa H. 2012. ES cell differentiation system recapitulates the establishment of imprinted gene expression in a cell-type-specific manner. Hum Mol Genet. 21:1391–1401.
Kohda T, Ishino F, Ogura A. 2006. Expression of imprinted genes in cloned mice. Methods Mol Biol. 348:237–246.
Kota SK, Lleres D, Bouschet T, Hirasawa R, Marchand A, Begon-Pescia C, Sanli I, Arnaud P, Journot L, Girardot M, et al. 2014. ICR noncoding RNA expression controls imprinting and DNA replication at the Dlk1-Dio3 domain. Dev Cell. 31:19–33.
Krueger F, Andrews SR. 2011. Bismark: a flexible aligner and methylation caller for Bisulfite-Seq applications. Bioinformatics. 27:1571–1572.

Kuwajima T, Nishimura I, Yoshikawa K. 2006. Necdin promotes GABAergic neuron differentiation in cooperation with Dlx homeodomain proteins. J Neurosci. 26:5383–5392.

Lancaster MA, Knoblich JA. 2014. Organogenesis in a dish: modeling development and disease using organoid technologies. Science. 345:1247125.

Latos PA, Stricker SH, Steenpass L, Pauler FM, Huang R, Senergin BH, Regha K, Koerner MV, Warczok KE, Unger C, et al. 2009. An in vitro ES cell imprinting model shows that imprinted expression of the Igf2r gene arises from an allele-specific expression bias. Development. 136:437–448.

Lehtinen MK, Zappaterra MW, Chen X, Yang YJ, Hill AD, Lun M, Maynard T, Gonzalez D, Kim S, Ye P, et al. 2011. The cerebrospinal fluid provides a proliferative niche for neural progenitor cells. Neuron. 69:893–905.

Livesey MR, Magnani D, Hardingham GE, Chandran S, Wyllie DJ. 2015. Functional properties of in vitro excitatory cortical neurons derived from human pluripotent stem cells. J Physiol. doi:10.1113/JP270660 (Epub ahead of print).

Luedi PP, Dietrich FS, Weidman JR, Bosko JM, Jirtle RL, Hartemink AJ. 2007. Computational and experimental identification of novel human imprinted genes. Genome Res. 17:1723–1730.

Lund RJ, Narva E, Lahesmaa R. 2012. Genetic and epigenetic stability of human pluripotent stem cells. Nat Rev Genet. 13:732–744.

Ma H, Morey R, O'Neil RC, He Y, Daughtry B, Schultz MD, Hariharan M, Nery JR, Castanon R, Sabatini K, et al. 2014. Abnormalities in human pluripotent cells due to reprogramming mechanisms. Nature. 511:177–183.

Mackay DJ, Callaway JL, Marks SM, White HE, Acerini CL, Boonen SE, Dayanikli P, Firth HV, Goodship JA, Haemers AP, et al. 2008. Hypomethylation of multiple imprinted loci in individuals with transient neonatal diabetes is associated with mutations in ZFP57. Nat Genet. 40:949–951.

Maeda T, Higashimoto K, Jozaki K, Yatsuki H, Nakabayashi K, Makita Y, Tonoki H, Okamoto N, Takada F, Ohashi H, et al. 2014. Comprehensive and quantitative multilocus methylation analysis reveals the susceptibility of specific imprinted differentially methylated regions to aberrant methylation in Beckwith-Wiedemann syndrome with epimutations. Genet Med. 16:903–912.

Mairet-Coello G, Tury A, Van Buskirk E, Robinson K, Genestine M, DiCicco-Bloom E. 2012. p57(KIP2) regulates radial glia and intermediate precursor cell cycle dynamics and lower layer neurogenesis in developing cerebral cortex. Development. 139:475–487.

Mariani J, Simonini MV, Palejev D, Tomasini L, Coppola G, Szekely AM, Horvath TL, Vaccarino FM. 2012. Modeling human cortical development in vitro using induced pluripotent stem cells. Proc Natl Acad Sci USA. 109:12770–12775.

Maupetit-Mehouas S, Montibus B, Nury D, Tayama C, Wassef M, Kota SK, Fogli A, Cerqueira Campos F, Hata K, Feil R, et al. 2016. Imprinting control regions (ICRs) are marked by mono-allelic bivalent chromatin when transcriptionally inactive. Nucleic Acids Res. 44:621–635.

Meissner A, Mikkelsen TS, Gu H, Wernig M, Hanna J, Sivachenko A, Zhang X, Bernstein BE, Nusbaum C, Jaffe DB, et al. 2008. Genome-scale DNA methylation maps of pluripotent and differentiated cells. Nature. 454:766–770.

Michelsen KA, Acosta-Verdugo S, Benoit-Marand M, Espuny-Camacho I, Gaspard N, Saha B, Gaillard A, Vanderhaeghen P. 2015. Area-specific reestablishment of damaged circuits in the adult cerebral cortex by cortical neurons derived from mouse embryonic stem cells. Neuron. 85:982–997.

Mueller OT, Coovadia A. 2008. Gene symbol: UBE3A. Disease: Angelman syndrome. Hum Genet. 124:304.

Nestor CE, Ottaviano R, Reinhardt D, Cruickshanks HA, Mjoseng HK, McPherson RC, Lentini A, Thomson JP, Dunican DS, Pennings S, et al. 2015. Rapid reprogramming of epigenetic and transcriptional profiles in mammalian culture systems. Genome Biol. 16:11.

Nicholas CR, Chen J, Tang Y, Southwell DG, Chalmers N, Vogt D, Arnold CM, Chen YJ, Stanley EG, Elefanty AG, et al. 2013. Functional maturation of hPSC-derived forebrain interneurons requires an extended timeline and mimics human neural development. Cell Stem Cell. 12:573–586.

Park Y, Figueroa ME, Rozek LS, Sartor MA. 2014. MethylSig: a whole genome DNA methylation analysis pipeline. Bioinformatics. 30:2414–2422.

Pick M, Stelzer Y, Bar-Nur O, Mayshar Y, Eden A, Benvenisty N. 2009. Clone- and gene-specific aberrations of parental imprinting in human induced pluripotent stem cells. Stem Cells. 27:2686–2690.

Plasschaert RN, Bartolomei MS. 2015. Tissue-specific regulation and function of Grb10 during growth and neuronal commitment. Proc Natl Acad Sci USA. 112:6841–6847.

Prickett AR, Oakey RJ. 2012. A survey of tissue-specific genomic imprinting in mammals. Mol Genet Genomics. 287:621–630.

Roadmap Epigenomics C, Kundaje A, Meuleman W, Ernst J, Bilenky M, Yen A, Heravi-Moussavi A, Kheradpour P, Zhang Z, Wang J, Ziller MJ, et al. 2015. Integrative analysis of 111 reference human epigenomes. Nature. 518:317–330.

Rothbart SB, Dickson BM, Raab JR, Grzybowski AT, Krajewski K, Guo AH, Shanle EK, Josefowicz SZ, Fuchs SM, Allis CD, et al. 2015. An interactive database for the assessment of histone antibody specificity. Mol Cell. 59:502–511.

Rugg-Gunn PJ, Ferguson-Smith AC, Pedersen RA. 2007. Status of genomic imprinting in human embryonic stem cells as revealed by a large cohort of independently derived and maintained lines. Hum Mol Genet. 2:R243–R251.

Sansom SN, Hebert JM, Thammongkol U, Smith J, Nisbet G, Surani MA, McConnell SK, Livesey FJ. 2005. Genomic characterisation of a Fgf-regulated gradient-based neocortical protomap. Development. 132:3947–3961.

Shi Y, Kirwan P, Smith J, Robinson HP, Livesey FJ. 2012. Human cerebral cortex development from pluripotent stem cells to functional excitatory synapses. Nat Neurosci. 15:477–486, S471.

Sleutels F, Tjon G, Ludwig T, Barlow DP. 2003. Imprinted silencing of Slc22a2 and Slc22a3 does not need transcriptional overlap between Igf2r and Air. EMBO J. 22:3696–3704.

Stelzer Y, Shivalila CS, Soldner F, Markoulaki S, Jaenisch R. 2015. Tracing dynamic changes of DNA methylation at single-cell resolution. Cell. 163:218–229.

Sun Y, Dong Z, Jin T, Ang KH, Huang M, Haston KM, Peng J, Zhong TP, Finkbeiner S, Weiss WA, et al. 2013. Imaging-based chemical screening reveals activity-dependent neural differentiation of pluripotent stem cells. Elife. 2:e00508.

Takada T, Ebata T, Noguchi H, Keane TM, Adams DJ, Narita T, Shin IT, Fujisawa H, Toyoda A, Abe K, et al. 2013. The ancestor of extant Japanese fancy mice contributed to the mosaic genomes of classical inbred strains. Genome Res. 23:1329–1338.

Thiagarajan RD, Morey R, Laurent LC. 2014. The epigenome in pluripotency and differentiation. Epigenomics. 6:121–137.

Tran DA, Bai AY, Singh P, Wu X, Szabo PE. 2014. Characterization of the imprinting signature of mouse embryo fibroblasts by RNA deep sequencing. Nucleic Acids Res. 42:1772–1783.

Tury A, Mairet-Coello G, DiCicco-Bloom E. 2012. The multiple roles of the cyclin-dependent kinase inhibitory protein p57(KIP2) in cerebral cortical neurogenesis. Dev Neurobiol. 72:821–842.

van de Leemput J, Boles NC, Kiehl TR, Corneo B, Lederman P, Menon V, Lee C, Martinez RA, Levi BP, Thompson CL, et al. 2014. CORTECON: a temporal transcriptome analysis of in vitro human cerebral cortex development from human embryonic stem cells. Neuron. 83:51–68.

Vandesompele J, De Preter K, Pattyn F, Poppe B, Van Roy N, De Paepe A, Speleman F. 2002. Accurate normalization of real-time quantitative RT-PCR data by geometric averaging of multiple internal control genes. Genome Biol. 3:RESEARCH0034.

Wang K, Li M, Hakonarson H. 2010. ANNOVAR: functional annotation of genetic variants from high-throughput sequencing data. Nucleic Acids Res. 38:e164.

Wang X, Clark AG. 2014. Using next-generation RNA sequencing to identify imprinted genes. Heredity (Edinb). 113:156–166.

Wang X, Soloway PD, Clark AG. 2011. A survey for novel imprinted genes in the mouse placenta by mRNA-seq. Genetics. 189:109–122.

Wang X, Sun Q, McGrath SD, Mardis ER, Soloway PD, Clark AG. 2008. Transcriptome-wide identification of novel imprinted genes in neonatal mouse brain. PLoS ONE. 3:e3839.

Wilkinson LS, Davies W, Isles AR. 2007. Genomic imprinting effects on brain development and function. Nat Rev Neurosci. 8:832–843.

Ying QL, Nichols J, Chambers I, Smith A. 2003. BMP induction of Id proteins suppresses differentiation and sustains embryonic stem cell self-renewal in collaboration with STAT3. Cell. 115:281–292.

Ying QL, Wray J, Nichols J, Batlle-Morera L, Doble B, Woodgett J, Cohen P, Smith A. 2008. The ground state of embryonic stem cell self-renewal. Nature. 453:519–523.